ADVANCED FUNCTIONAL MATERIALS
www.afm-journal.de

Revealing the Impact of F4-TCNQ as Additive on Morphology and Performance of High-Efficiency Nonfullerene Organic Solar Cells

Yuan Xiong, Long Ye, Abay Gadisa, Qianqian Zhang, Jeromy James Rech, Wei You, and Harald Ade**

Fluorinated molecule 2,3,5,6-tetrafluoro-7,7,8,8-tetracyanoquinodimethane (F4-TCNQ) and its derivatives have been used in polymer:fullerene solar cells primarily as a dopant to optimize the electrical properties and device performance. However, the underlying mechanism and generality of how F4-TCNQ affects device operation and possibly the morphology is poorly understood, particularly for emerging nonfullerene organic solar cells. In this work, the influence of F4-TCNQ on the blend film morphology and photovoltaic performance of nonfullerene solar cells processed by a single halogen-free solvent is systematically investigated using a set of morphological and electrical characterizations. In solar cells with a high-performance polymer:small molecule blend FTAZ:IT-M, F4-TCNQ has a negligibly small effect on the molecular packing and surface characteristics, while it clearly affects the electronic properties and mean-square composition variation of the bulk. In comparison to the control devices with an average power conversion efficiency (PCE) of 11.8%, inclusion of a trace amount of F4-TCNQ in the active layer has improved device fill factor and current density, which has resulted into a PCE of 12.4%. Further increase in F4-TCNQ content degrades device performance. This investigation aims at delineating the precise role of F4-TCNQ in nonfullerene bulk heterojunction films, and thereby establishing a facile approach to fabricate highly optimized nonfullerene solar cells.

1. Introduction

Organic photovoltaic (OPV) has emerged as a promising technology for renewable energy generation, due to its viability for large-area manufacturing[1] through roll-to-roll printing technology using low-cost materials and eco-friendly solvents.[2–8] In a typical bulk-heterojunction OPV, a binary mixture of donor and acceptor molecule constitutes the photoactive layer, where charge generation and transport occur. In the quest of achieving high-efficiency OPVs, extensive efforts have been devoted to the design and synthesis of new conjugated polymers and nonfullerene molecule acceptors.[9–12] In addition to the materials innovations, manipulating the multiple morphology parameters such as molecular packing, molecular orientation, domain size, miscibility, and vertical composition distribution is also critical for the development of OPVs,[13,14] in particular for those based on nonfullerene acceptors.

The performance of binary systems is usually limited by the intrinsic properties (absorption, charge mobility) of the constituent materials. To overcome the intrinsic limitation of a binary mixture, a third component[15,16] is often introduced to enhance certain properties of OPVs. For instance, adding an absorber or sensitizer could significantly improve the light absorption and form an energetic cascade structure for more efficient charge creation. Unlike absorber materials, a fluorinated molecule 2,3,5,6-tetrafluoro-7,7,8,8-tetracyanoquinodimethane (F4-TCNQ) with poor optical absorption (**Figure 1**) has been recently used to optimize the electrical properties of polymer:fullerene films. It is noteworthy that the effects of small molecule F4-TCNQ generally depend on the systems and processing conditions and the precise role of F4-TCNQ is still under debate. For instance, a previous study[17] by Moulé and co-workers demonstrated that the F4-TCNQ additive had the tendency to remain in polar polymer S-P3MEET due to the strong binding force with poly(ethylene oxide) (PEO) side-chain of the polymer. Nevertheless, F4-TCNQ can diffuse out of the nonpolar polymer P3HT. Moreover, another study demonstrated that F4-TCNQ preferred to segregate to the air/liquid interface during the solvent drying process in P3HT:PCBM system.[18] In addition, Salleo group[19] suggested that the behavior of F4-TCNQ in unannealed and annealed P3HT:PCBM devices was different,

Y. Xiong, Dr. L. Ye, Dr. A. Gadisa, Prof. H. Ade
Department of Physics
Organic and Carbon Electronics Lab (ORaCEL)
North Carolina State University
Raleigh, NC 27695, USA
E-mail: lye4@ncsu.edu; hwade@ncsu.edu
Dr. Q. Zhang, J. J. Rech, Prof. W. You
Department of Chemistry
University of North Carolina at Chapel Hill
Chapel Hill, NC 27599, USA
The ORCID identification number(s) for the author(s) of this article can be found under https://doi.org/10.1002/adfm.201806262.

DOI: 10.1002/adfm.201806262

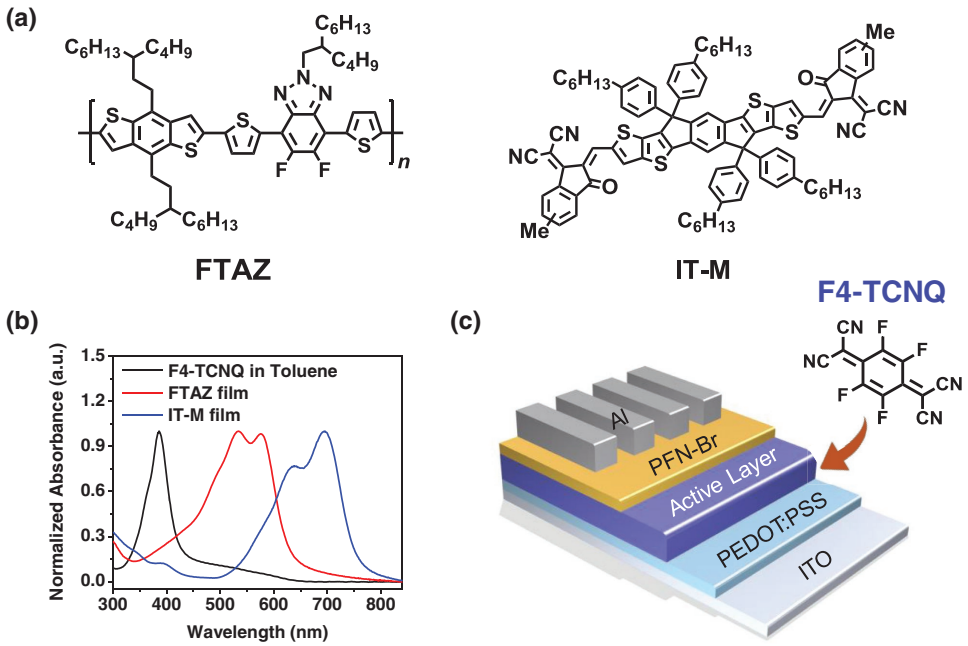

Figure 1. a) Molecular structures of photovoltaic materials (FTAZ and IT-M) used in this work; b) UV–Vis absorption spectra of the materials; c) Configuration of the devices and molecular structure of F4-TCNQ.

and the study suggested that the trade-off between trap filling, trap creation, and charge recombination leads to the performance enhancement by introducing ultralow amount (≈10^{-4} by weight) of F4-TCNQ. Furthermore, Zhang et al.[20] investigated that addition of low concentration of F4-TCNQ was able to improve the photoconductivity in PCDTBT:PCBM system. Yan et al.[21] later applied this strategy to a higher performance PTB7-Th:PCBM device. Overall, although the device performance can be optimized in most cases and comprehensive studies have been carried out, less attention has been paid to the polymer:fullerene morphology in the aforementioned studies. Until recently, we note that there is still some lack of knowledge about the impact of F4-TCNQ on the OPV morphology. Especially, the impact of F4-TCNQ on the nanoscale and mesoscale morphological and electrical properties of nonfullerene OPVs has seldom been studied.

In this study, we aim to fully understand the role of F4-TCNQ in the electrical, morphological, and photovoltaic properties of high performance nonfullerene organic solar cells. The model nonfullerene material system used is a recently reported combination FTAZ:IT-M[6] (Figure 1a), which was able to break the 10% efficiency benchmark by blade-coating in air using single halogen-free solvent, and this system and its derivatives (with only minor structure modifications) were widely studied in the community of organic solar cells and attracted significant attention (Table S1, Supporting Information). For the optimized FTAZ:IT-M devices, our results demonstrate that enhanced fill factor (FF) (≈71%) and short-circuit current density (18.7 mA cm^{-2}) can be realized by simply loading 0.02 mg mL^{-1} of F4-TCNQ in FTAZ:IT-M–based solar cells. This leads to a high power conversion efficiency (PCE) value of ≈12.4% for FTAZ:IT-M–based devices. To investigate the microstructure evolution of these nonfullerene solar cells with varied amount of F4-TCNQ, we performed comprehensive characterizations by introducing different optoelectrical and morphological techniques. Our electrical results indicated that the effect of F4-TCNQ was on the bulk rather than the interface. Morphological measurements suggested that the vertical composition and molecular packing are not affected much by the addition of F4-TCNQ, while the mean-square composition variation[13,22] is dramatically altered by the amount of F4-TCNQ. Very small levels of F4-TCNQ have no impact on the photovoltaic device performance, suggesting that the trap density modulation in this system is negligible, possibly due to a smaller electronic disorder in nonfullerene systems over fullerene systems. Moreover, highly consistent results were observed in a completely different nonfullerene pair comprising PTB7-Th and EH-IDTBR,[23,24] which is another widely used system in the field of nonfullerene OPVs. This study thus provides an in-depth understanding of the mechanism of F4-TCNQ and its effect on the nanoscale and mesoscale morphology of nonfullerene OPVs.

2. Results and Discussion

2.1. Photovoltaic Performance

To understand the impact of F4-TCNQ on device performance, we fabricated a set of bulk heterojunction (BHJ) solar cells by only varying the concentration of F4-TCNQ in a conventional configuration (Figure 1c). We used a halogen-free solvent toluene as the host solvent and kept the FTAZ to IT-M weight ratio at 1:1 for all devices, which is fully consistent with the protocols reported in our prior work[6]. Specifically, toluene with various concentrations of F4-TCNQ (0-0.05 mg mL^{-1}) was used

Table 1. Photovoltaic performances of FTAZ:IT-M solar cells with various concentrations of F4-TCNQ toluene solutions.

F4-TCNQ [mg mL^{-1}][a)]	V_{oc} [mV]	J_{sc} [mA cm^{-2}]	FF [%]	PCE [%]
0	965 ± 6	17.80 ± 0.5	68.69 ± 0.7	11.89 ± 0.15
0.001	967 ± 1	18.03 ± 0.1	68.30 ± 0.4	11.89 ± 0.06
0.004	960 ± 2	18.14 ± 0.2	68.13 ± 0.8	11.93 ± 0.19
0.01	957 ± 3	18.08 ± 0.2	70.08 ± 0.5	12.12 ± 0.20
0.02	954 ± 6	18.19 ± 0.3	70.41 ± 0.3	12.22 ± 0.12
0.03	923 ± 3	17.44 ± 0.2	57.14 ± 1.1	9.21 ± 0.26
0.05	907 ± 4	16.33 ± 0.3	55.88 ± 1.1	8.28 ± 0.28

[a)]Toluene with different concentrations were used for dissolving the FTAZ:IT-M blends.

to dissolve the FTAZ:IT-M blends. All photovoltaic devices with similar film thickness (≈110 nm) were characterized and the corresponding photovoltaic parameters are displayed in **Table 1**. The performance of the reference device (without F4-TCNQ) is quite comparable to the reported value.

We noted that adding an ultralow amount (0.001–0.004 mg mL^{-1}) of F4-TCNQ cannot affect the device performance. The effects of F4-TCNQ start at the additive concentrations approaching 0.01 mg mL^{-1}, and an optimum condition leading to the highest device efficiency was achieved at a F4-TCNQ concentration of 0.02 mg mL^{-1}. With the incorporation of 0.02 mg mL^{-1} F4-TCNQ into the host blend, the average J_{sc} increased from 17.80 to 18.19 mA cm^{-2}, and a slight improvement of FF (from 68.69% to 70.41%) was observed, leading to an overall enhanced PCE of 12.22%. Conversely, OPV devices with higher concentrations (>0.02 mg mL^{-1}) of F4-TCNQ exhibit reduced overall PCE due to the loss of V_{oc}, J_{sc}, and FF. **Figure 2**a and Figure S1 in the Supporting Information show the typical current density versus voltage (*J*–*V*) characteristics of the devices with various F4-TCNQ contents under simulated air mass (AM) 1.5G solar irradiation (100 mW cm^{-2}). From the external quantum efficiency (EQE) (Figure 2b), we note that 0.02 mg mL^{-1} F4-TCNQ cells show increased spectral response in the 400–600 nm region. As a result, the improved current indicates that F4-TCNQ might be beneficial to the charge extraction and transport in the FTAZ:IT-M system. Understanding the actual mechanism requires in-depth investigations of the electrical and morphological properties.

2.2. Surface Characteristics

As reported in the literature, generally, F4-TCNQ either changes the charge recombination and transport in the BHJ films or segregates to the interface between the active layer and electrode to improve the interface contact. To establish a thorough understanding of the effect of F4-TCNQ on the electrical, morphological, and photovoltaic properties, we purposely choose the three representative devices (with 0 mg mL^{-1}, 0.02 mg mL^{-1}, and 0.05 mg mL^{-1} F4-TCNQ) for the subsequent experiments using a set of techniques. At first, contact angle measurement was utilized to estimate the surface composition of these blend films. Diiodomethane droplets on top of the blend layers with 0 mg mL^{-1}, 0.02 mg mL^{-1}, and 0.05 mg mL^{-1} F4-TCNQ were monitored with a digital camera during deposition and fluid evaporation process, and the left and right contact angles were recorded as shown in Figure S2 in the Supporting Information. Similar contact angles of around 47° were achieved, which indicates no distinctively different interfacial tensions of these three films through the inclusion of the F4-TCNQ. Furthermore, we also analyzed the vertical composition profiles by employing depth profiling with secondary ion mass spectroscopy (SIMS). The SIMS results shown in Figure 2c also verify that the vertical composition is not substantially changed.

We then carried out electrochemical impedance spectroscopy (EIS) analysis[26–30] to gain more insight into electrical characteristics of the solar cells by introduction of F4-TCNQ. Usually, the typical Nyquist plots of OPVs feature two partial semicircular arcs: one arc in the high-frequency region is associated to the charge transport and extraction at the electrode interfaces, while the other arc in the low-frequency region represents the characteristics of charge recombination in the bulk of the BHJ films. Therefore, this method can be used to effectively identify the response from different layers. The impedance response of 0.02 mg mL^{-1}, 0.05 mg mL^{-1} devices as well as the reference FTAZ:IT-M devices were measured by impedance spectroscopy module integrated in a commercial setup (PAIOS from FLUXiM) at short-circuit conditions under varying illumination from 0% to 100% in the frequency range from 10^6 to 10 Hz (Figure S3,

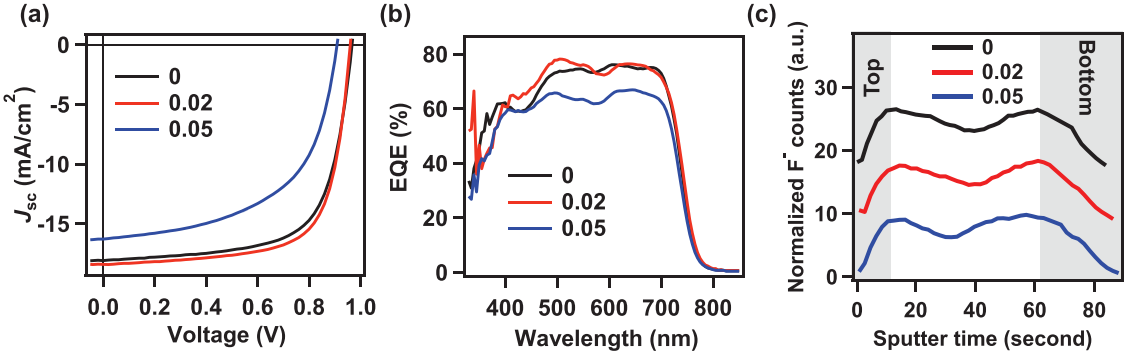

Figure 2. a) *J*–*V* characteristics of FTAZ:IT-M solar cells with 0 mg mL^{-1}, 0.02 mg mL^{-1}, and 0.05 mg mL^{-1} F4-TCNQ under solar simulator illumination (100 mW cm^{-2}). b) Corresponding EQE curves of the devices shown in (a). c) Plots of the count of F$^-$ segment versus SIMS sputtering time (second).

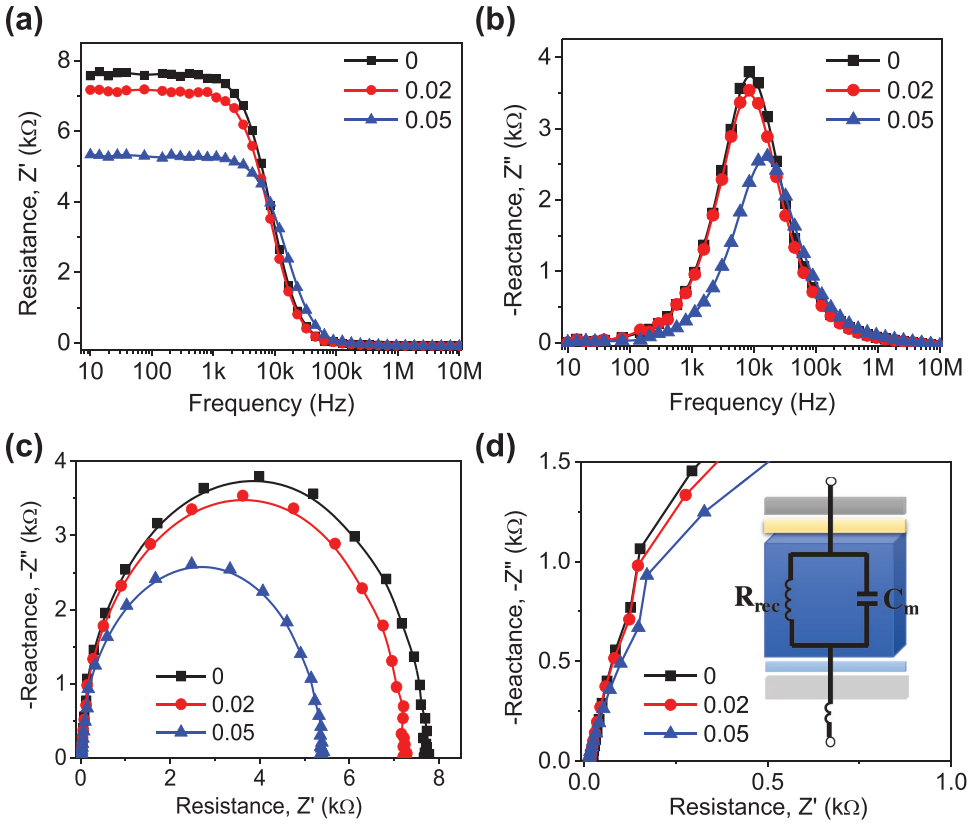

Figure 3. Impedance response of FTAZ:IT-M devices with various contents of F4-TCNQ at short-circuit conditions and the maximum 100% light intensity illumination conditions. Resistance a), Reactance b) as a function of the frequency, and the corresponding Nyquist plot c). d) Impedance response at the high-frequency range and the simplified equivalent circuit model of the FTAZ:IT-M solar cells.

Supporting Information). In the Nyquist plots of three different devices, we found only one obvious semicircle and the response from the interfacial layer at high-frequency region (**Figure 3**d) is negligibly small and invariant with device type, indicating that the F4-TCNQ has no effect on the device interfaces but rather affects the bulk of the BHJ blend. The latter observation is in agreement with the contact angle and SIMS measurements.

Based on the impedance response under the operating condition presented in Figure 3, the corresponding fitted photoelectrochemical parameters according to the simplified equivalent circuit model in Figure 3d are listed in **Table 2**. In the equivalent circuit, the recombination resistance (R_{rec}) represents all the photogenerated charges whether they are extracted to the electrodes or recombine in the Bulk.[27,31] For the 0.02 mg mL^{-1} F4-TCNQ device, we note that its R_{rec} is slightly lower than that of the reference sample. This implies that 0.02 mg mL^{-1} F4-TCNQ device with relatively higher mobile charge carrier concentration also exhibits a lower bimolecular recombination rate. This observation agrees with the higher J_{sc} of 0.02 mg mL^{-1} F4-TCNQ devices. On the other hand, the 0.02 mg mL^{-1} F4-TCNQ devices exhibit higher chemical potential (C_m), which together with the R_{rec} defines the lifetime of the charge carriers τ_{ave} ($\tau_{ave} = R_{rec} \times C_m$). τ_{ave} can also be directly approximated from the frequency (f) at which the reactance reaches its peak value.[32] The results (see Table 2) show that the enhanced chemical potential in the 0.02 mg mL^{-1} F4-TCNQ devices resulted into increased charge carrier lifetime compared with the reference devices, while the 0.05 mg mL^{-1} F4-TCNQ devices show the shortest lifetime under the same condition. It again confirms that the addition of 0.02 mg mL^{-1} F4-TCNQ prolongs the charge carrier lifetime, which leads to a better chance that carriers reach the electrode enabling higher yield of J_{sc}.

Table 2. The fitted parameters of each element in the equivalent model of FTAZ:IT-M devices with various concentrations of F4-TCNQ.

F4-TCNQ Concentration [mg mL^{-1}]	f [Hz]	R_{rec} [kΩ]	C_m [F]	τ_{avg} [ms]
0	8794	7.65	2.28	17.44
0.02	8490	7.15	2.48	17.73
0.05	15351	5.32	1.83	9.74

2.3. Recombination Dynamics

To gain more insights into the charge transport and recombination mechanisms leading to the photovoltaic performance improvements in FTAZ:IT-M devices with a moderate fraction of F4-TCNQ, we studied the light intensity–dependent photovoltaic characteristics.[33] For the light-dependence relation shown in **Figure 4**a, recombination at open-circuit voltage can be analyzed based on the relation $V_{oc} = nkT/q \ln(J_{sc}/J_s)$, where k is the Boltzmann constant, T is temperature, q is the elementary charge,

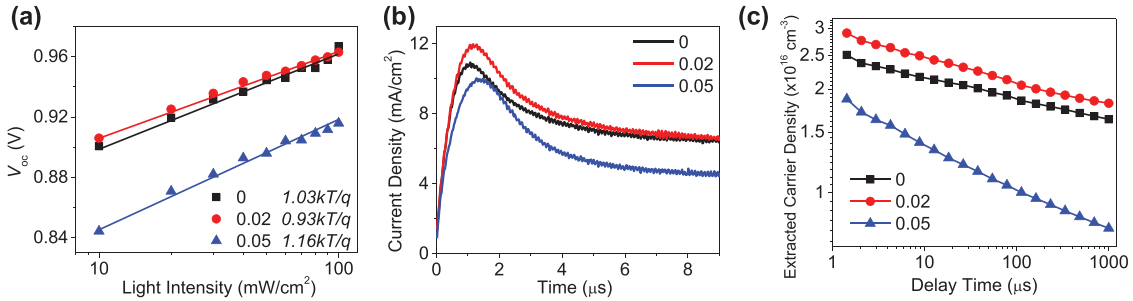

Figure 4. Light intensity–dependent V_{oc} characteristics a), CELIV result at 2 μs delay time b), and extracted carrier density versus delay time c) of the three representative devices using 0 mg mL^{-1}, 0.02 mg mL^{-1} and 0.05 mg mL^{-1} F4-TCNQ toluene solution, respectively.

J_s is the saturation current density, and n is the ideality factor, which is subject to the exact recombination mechanism, namely n approaching unity signifies the dominance of bimolecular recombination while values close to 2 are achieved in devices operating under the influence of monomolecular or trap-assisted recombination.[34] Fits to the experimental data V_{oc} against light intensity give slopes of 1.03 kT/q, 0.93 kT/q, and 1.16 kT/q, as the content of F4-TCNQ varies from 0 to 0.05 mg mL^{-1}, respectively. Therefore, the results reveal the reduction of the trap-assisted monomolecular recombination in the 0.02 mg mL^{-1} F4-TCNQ device. The severe degradation of the V_{oc} of the 0.05 mg mL^{-1} doped device could be attributed to its higher trap concentrations, which might be created by the dopant ions.

To probe charge carrier mobility and recombination kinetics in more details, we employed photoinduced charge carrier extraction by linearly increasing voltage (photo-CELIV) technique,[35–38] which enables characterization of charge dynamics in operational photovoltaic devices (See Supporting Information for details of analysis). Figure 4b exhibits the photo-CELIV characteristics recorded at a delay time of 2 μs. The fastest charge carrier mobility extracted from the photo-CELIV data was found to be 3.45×10^{-4}, 3.77×10^{-4}, and 3.25×10^{-4} cm^2 V^{-1} s^{-1} for the 0, 0.02, and 0.05 mg mL^{-1} devices, respectively, extracted charge carrier densities follow the same trend as shown in **Table 3**. Overall, the results suggest again that the introduction of 0.02 mg mL^{-1} F4-TCNQ indeed enhances the mobility and density of the photoinduced charges carriers, consequently resulting in enhanced FF and J_{sc}.

Further investigation of charge carrier loss was carried out by exploring charge carrier dynamics of the devices by varying the delay time between the light-pulse and the extracting voltage ramp. The CELIV current of FTAZ:IT-M cells with varying content of F4-TCNQ as a function of the delay time is shown in Figure S5 in Supporting Information. The density of the charge carriers (n) under different delay time (Figure 4c) reveals that though a universal decrement of charge density with delay time is observed, devices comprising 0.02 mg mL^{-1} F4-TCNQ encountered the relatively slow charge carrier loss. Hence, the addition of F4-TCNQ suppresses recombination in fully operational devices if its concentration is carefully tuned.

Table 3. Charge carrier mobility (μ) and extracted charge carrier density (n) of FTAZ:IT-M–based OPVs. Values were estimated from photo-CELIV measurements.

F4-TCNQ Concentration [mg mL^{-1}]	μ [cm^2 V^{-1} s^{-1}]	n [cm^{-3}]
0	3.45×10^{-4}	2.38×10^{16}
0.02	3.77×10^{-4}	2.76×10^{16}
0.05	3.25×10^{-4}	1.71×10^{16}

2.4. Molecular Packing and Mesoscale Morphology

Having understood the impact of F4-TCNQ on device operation, we now search for details of the exact mechanism(s) underlying the role of these additives in charge generation, transport, and recombination based on analysis of the BHJ morphology. To understand the change in the amount of F4-TCNQ on the molecular packing or nanoscale ordering of FTAZ:IT-M blend films, the OPV films are probed with a synchrotron diffraction technique, grazing incidence wide-angle X-ray scattering (GIWAXS).[39] The 2D GIWAXS patterns and the corresponding in-plane (IP) and out-of-plane (OOP) line-cut profiles of the blend films are shown in **Figure 5**. The three blend films all showed apparent π–π (010) stacking peaks at $q = 1.75$ Å^{-1} in the OOP direction and lamellar (100) diffraction peaks with $q = 0.30$ Å^{-1} in the IP direction. The diffraction features and distribution functions for (100) peaks are analogous to these three blend films (see Figure S6, Supporting Information), indicative of a highly similar packing at the molecular level. Additionally, we performed multipeak fitting of OOP (010) peaks at $q \approx 1.7$ Å^{-1} of FTAZ:IT-M blends with different amount of F4-TCNQ. The detailed analysis and associated results are shown in Figure S7 and Table S2 in the Supporting Information. It was clear that the (010) coherence lengths are very comparable. Accordingly, molecular packing is not a major factor contributing to the difference in device performance.

Next, the degree of phase separation in the blend films was explored with resonant soft X-ray scattering (R-SoXS).[40,41] From the 1D scattering profiles shown in Figure 5d, we found that the scattering peaks are located at similar location ($q = 0.25$ nm^{-1}), indicating comparable long period (or center-to-center domain spacing). The mean-square composition variation, as defined by the integral of the scattering profiles over the length scale probed, is a widely used indicator related to the average domain purity of OPV blends. Compared to the reference device, the 0.02 mg mL^{-1} F4-TCNQ device shows a much larger composition variation while the 0.05 mg mL^{-1} device exhibits a much lower composition

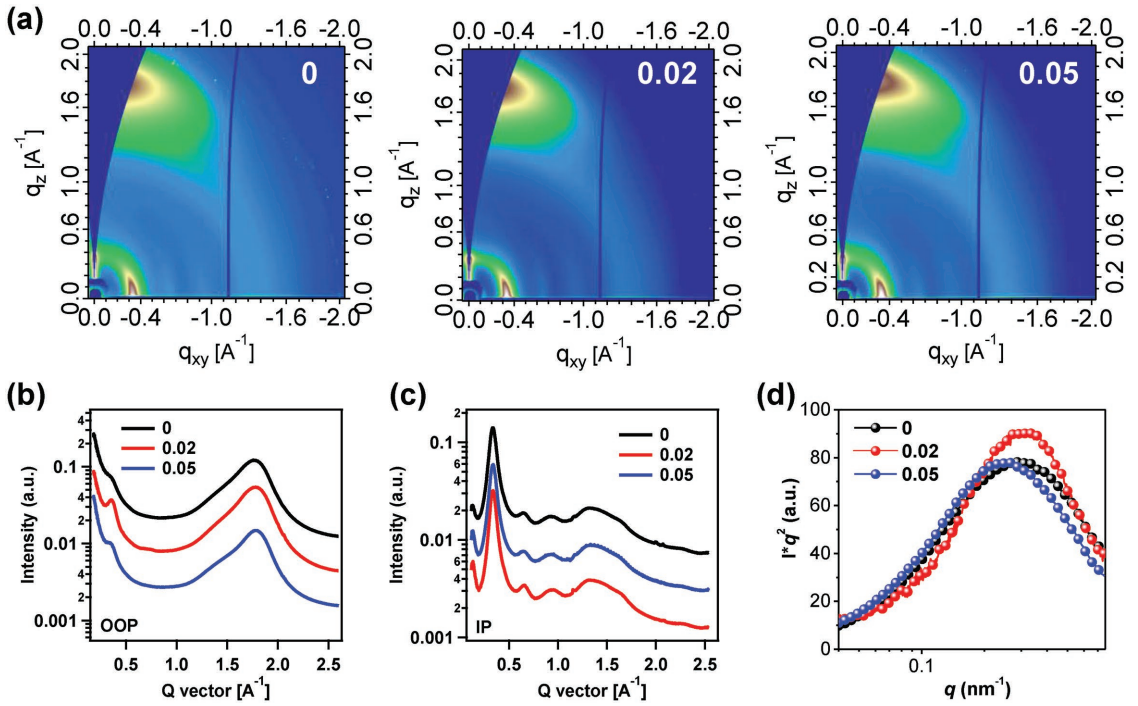

Figure 5. a) GIWAXS 2D pattern, b) out-of-plane, and c) in-plane of FTAZ and IT-M with various content of F4-TCNQ, d) Lorentz-corrected scattering profiles from azimuthally averaged R-SoXS images of FTAZ:IT-M profiles at a photon energy of ≈284 eV.

variation. To make a quantitative comparison, we set the composition variation of 0.02 mg mL^{-1} as 1 and the corresponding values for the 0 mg mL^{-1} and 0.05 mg mL^{-1} F4-TCNQ devices are 0.96 and 0.88, respectively.

2.5. Discussion

This investigation has shown that inclusion of a trace amount of F4-TCNQ in a highly efficient nonfullerene organic solar cell based on FTAZ:IT-M clearly improves device photovoltaic properties. To the best of our knowledge, this is the first work that shows the underlying mechanism of F4-TCNQ in nonfullerene OPV systems. On the basis of contact angle, SIMS, nuclear magnetic resonance spectroscopy (see Figure S8, Supporting Information), and UV–Vis absorption results (see Figure S9, Supporting Information), F4-TCNQ neither enriches device interfaces nor resides in the bulk of the BHJ blend. The combined EIS and Photo-CELIV techniques used clearly suggest that the addition of 0.02 mg mL^{-1} F4-TCNQ optimizes the charge generation and transport. This introduction not only prolongs the charge carrier lifetime but also enhances the mobility and density of the photo-induced charges carriers, consequently resulting in enhanced FF and J_{sc}. As a consequence, an enhanced PCE up to 12.4% is achieved in the OPV devices based on the FTAZ:IT-M combination.

Furthermore, our morphological data based on image/depth methods and scattering techniques (GIWAXS and R-SoXS) confirm the EIS results and show that the addition of F4-TCNQ indeed affects several morphological properties of the BHJ. Contact angle, SIMS, and GIWAXS measurements together reveal that F4-TCNQ does not change the molecular packing, surface composition, and vertical composition profiles. Domain spacing also remains unchanged from R-SoXS observations. As a result, the morphological origin of the better performance of 0.02 mg mL^{-1} devices can be ascribed to the higher mean-square composition variation, which scales with the average phase purity of mixed domains. Since the addition of F4-TCNQ can tune the mesoscale morphology, F4-TCNQ serves here as a morphological aid in the nonfullerene solar cells rather than an electrical dopant as suggested by previous studies on polymer:fullerene systems.

After successfully improving the device performance of FTAZ:IT-M by introducing 0.02 mg mL^{-1} F4-TCNQ additive due to the enhanced charge carrier lifetime, mobility, and phase purity, we further investigated another and representative system PTB7-Th:EH-IDTBR (molecular structures are shown in Figure S10, Supporting Information) to test the general nature of this approach. First, we fabricated the BHJ devices with different concentration of F4-TCNQ (0, 0.02, and 0.05 mg mL^{-1}). Figure S11 in the Supporting Information and **Table 4** present the photovoltaic characteristics of the

Table 4. Photovoltaic performances of PTB7-Th:EH-IDTBR solar cells with various amounts of F4-TCNQ.

F4-TCNQ concentration [mg mL^{-1}]	V_{oc} [mV]	J_{sc} [mA cm^{-2}]	FF [%]	PCE [%]
0	1018 ± 4	15.90 ± 0.36	65.65 ± 0.62	10.63 ± 0.19
0.02	1002 ± 2	16.55 ± 0.17	66.37 ± 0.19	11.01 ± 0.15
0.05	981 ± 4	15.62 ± 0.13	59.03 ± 0.59	9.04 ± 0.14

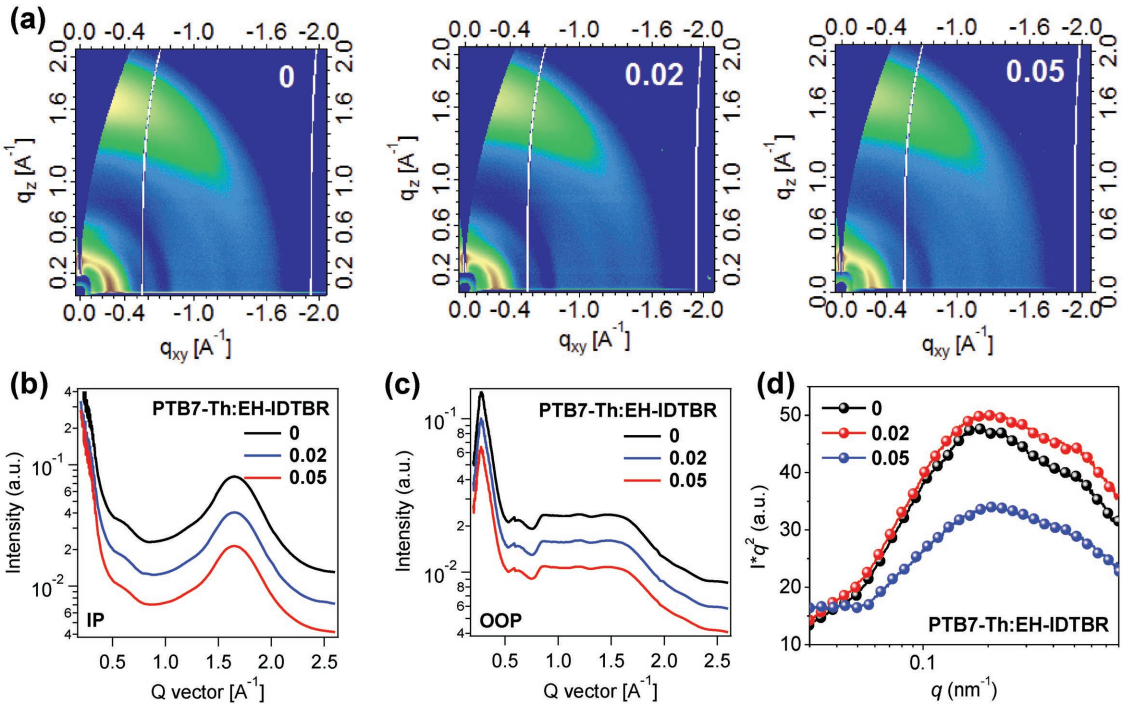

Figure 6. a) GIWAXS 2D patterns, b) in-plane, and c) out-of-plane of PTB7-Th and EH-IDTBR with various content of F4-TCNQ, d) Lorentz-corrected R-SoXS profiles from azimuthally averaged R-SoXS images of PTB7-Th:EH-IDTBR films at a photon energy of ≈284 eV.

devices under 1 sun illumination. It can be readily observed that the 0.02 mg mL^{-1} additive in PTB7-Th:EH-IDTBR solar cell induces a considerable improvement of J_{sc} and FF, thus achieving an enhanced PCE over 11%. Moreover, **Figure 6**a–c indicates again that the molecular packing is still not a major factor contributing to the difference in PTB7-Th:EH-IDTBR device performance, while the mesoscale morphology (Figure 6d) shows a similar trend as presented earlier in the FTAZ:IT-M case. This consistent observation in two representative nonfullerene systems corroborates the robustness of our finding that 0.02 mg mL^{-1} F4-TCNQ improves the phase purity of nonfullerene OPVs. The morphology-efficiency relationship revealed in our study, therefore, provides a new insight into the effects of F4-TCNQ additive on nonfullerene solar cells.

3. Conclusions

In summary, we have comprehensively investigated the effect of a fluorinated molecule F4-TCNQ on morphology and performance of high-efficiency nonfullerene solar cells. The photovoltaic behaviors based on FTAZ:IT-M devices can be improved by introducing 0.02 mg mL^{-1} F4-TCNQ with the best PCE approaching 12.4%. By means of the surface contact angle and vertical microstructure profiles, we have clearly observed no difference in the molecular composition of the interface. The light intensity–dependent impedance response not only confirms the observations of the surface characterization but also reveals that moderate content of F4-TCNQ prolongs the charge carrier lifetime. Together with the measurement of light-dependent V_{oc}, we found that higher concentrations of F4-TCNQ create more traps in the bulk, leading to a poor performance. In addition, Photo-CELIV measurement allows a successful analysis of charge carrier recombination dynamics, which demonstrates that the superior FTAZ:IT-M devices with 0.02 mg mL^{-1} F4-TCNQ are associated with a higher charge carrier density, charge carrier mobility, and relatively lower charge recombination rate. Furthermore, the morphological measurements provide us more insights on the microstructure of these blends. Molecular packing and domain spacing remain largely unchanged after adding F4-TCNQ, while 0.02 mg mL^{-1} additive results in a higher mean-square composition variation. It suggests that the addition of F4-TCNQ can tune the mesoscale morphology. The additional PTB7-Th:EH-IDTBR system further confirms our interpretation.

Based on the results of FTAZ:IT-M and PTB7-Th:EH-IDTBR systems, we are able to conclude that the enhanced performance by adding F4-TCNQ can be ascribed to not only the higher charge lifetime, charge carrier density, and mobility, but also the higher mean-square composition variation. This work frames an insightful guideline into the potential of functional additives, such as F4-TCNQ, for improving the photovoltaic characteristics of high-efficiency nonfullerene solar cells.

4. Experimental Section

Materials: FTAZ was prepared following the reported method.[42] PTB7-Th, EH-IDTBR, and IT-M were purchased from 1-Material Inc. 2,3,5,6-Tetrafluoro-7,7,8,8-tetracyanoquinodimethane (>97%) (F4-TCNQ) was purchased from Sigma-Aldrich.

Device Fabrication and Characterizations: Conventional polymer solar cells were fabricated on indium tin oxide (ITO)-coated (≈15 Ω sq^{-1}) glass substrates, which were cleaned sequentially in soap deionization water, deionization water, acetone, and isopropanol for 30 min each step. After an ultraviolet/ozone treatment for 10 min, poly(3,4-ethylenedioxythiophene):poly(styrenesulfonate) (PEDOT:PSS) (Baytron P VP Al 4083) layer was spin-coated at a spin-coating rate of 4000 rpm to form ≈30 nm thin film, followed by annealing at 150 °C for 10 min. FTAZ:IT-M solution (D/A ratio 1:1, total concentration 10 mg mL^{-1}) was prepared in toluene; PTB7-Th:EH-IDTBR solution (D/A ratio 1:1.5, total concentration 25 mg mL^{-1}) was prepared in chlorobenzene (CB). Meanwhile, F4-TCNQ was dissolved in toluene or CB with certain concentrations (0, 0.02, 0.05 mg mL^{-1}, etc) and then used as solvents to dissolve the active layer blends before the casting. Both solutions were stirred on a hot plate to 80 °C for at least 5 h to completely dissolve the polymers. Next in the N_2-filled glovebox, the FTAZ:IT-M active layers were cast at the spin speed of 1000 rpm for 60 s resulting in a thickness of about 110 nm, while the PTB7-TH:EH-IDTBR solutions were spun cast at the speed of 2000 rpm for 60 s to form about 100-nm-thick films. Furthermore, all blend films were annealed at 150 °C for 10 min in glovebox. Then PFN-Br solution was cast to be used as the cathode interlayer (≈5 nm). After that, they were directly transferred to a metal deposition system. Al (100 nm) was sequentially deposited onto the active layers via a mask (6.9 mm^2) under 1×10^{-6} Pa vacuum. The current density–voltage (*J*–*V*) characteristics of the PSCs were measured in the glovebox on a computer-controlled Keithley 2400 Source-Measure unit. The device photocurrent was measured under AM1.5G (100 mW cm^{-2}) using a Newport solar simulator, which was calibrated using a standard Si photodiode detector (with KG5 filter) for light intensity calibration. For each device, there were four independent working devices per substrate (1.5 cm × 1.5 cm), and each was illuminated through a metal aperture (6.9 mm^2). EQE measurements were performed using a Newport EQE system equipped with a standard Si diode as a reference. The contact angles of water were determined using a goniometer using Diiodomethane (99% purity, from Aldrich) droplets at room temperature at a constant volume of 5 µL. A total of eight static measurements were analyzed and averaged for each film. The SIMS was carried out in an ION TOF TOF-SIMS 5. Dual-beam dynamic SIMS mode was used to provide high-depth resolution and chemical resolution simultaneously, where Bi^+ was employed as the primary ion and Cs^+ was employed as a sputtering source. The sputtering parameters were set to be the same for all samples.

PAIOS: The EIS and Photo-CELIV measurements were performed in the air, while the polymer solar cells were encapsulated by epoxy to avoid the degradation under the explosion of oxygen and moisture. In the photo-CELIV measurements, a light-pulse created charges inside of the solar cells, which were then extracted by a linearly increasing voltage pulse (*U*) with a slope of $A = U/t_{tr}$, where t_{tr} is the transient time. The schematic illustration of the photo-CELIV method is shown in Figure S4 in the Supporting Information. The charge carrier mobility was calculated from the equation: $\mu = 2kd^2/3At_{max}^2(1 + 0.36\Delta j/j_0)$ and the number of extracted charge carriers was evaluated by integrating the current overshoot on top of the displacement current.[43]

GIWAXS: Grazing-incidence wide-angle X-ray scattering (GIWAXS) was conducted at beamline 7.3.3 at the Advanced Light Source, Lawrence Berkeley National Laboratory. Samples were prepared on top of Si substrates. The 10 keV X-ray beam was incident at a grazing angle of 0.13, which maximized the scattering intensity from the active layers. A 2M Pilatus 2D detector was used to collect the scattering patterns. All measurements were conducted under a helium atmosphere to reduce air scattering.

R-SoXS: Resonant soft X-ray scattering (R-SoXS) was performed at the beamline 11.0.1.2,[40,41] Advanced Light Source, Lawrence Berkeley National Lab. All measurements were conducted under high vacuum (1×10^{-7} torr) to reduce the air absorption of soft X-rays. Active layers were flushed with deionized water and transferred onto Si_3N_4 substrates. The scattering patterns were collected by a 2048 × 2048 pixel charge-coupled device (CCD) detector.

Supporting Information

Supporting Information is available from the Wiley Online Library or from the author.

Acknowledgments

This research was carried out at NCSU with supports from UNC-GA Research Opportunity Initiative grant and the NSF INFEWS grant CBET 1639429. Q. Z. and W. Y. were supported by the ONR grant N000141410221 and NSF (No. DMR-1507249). Beamlines 7.3.3 and 11.0.1.2 at the Advanced Light Source are supported by the Director of the Office of Science, Office of Basic Energy Sciences, of the U.S. Department of Energy under Contract No. DE-AC02-05CH11231. Use of the Advanced Photon Source was supported by the U.S. Department of Energy, Office of Science, Office of Basic Energy Sciences, under Contract DE-AC02-06CH11357. We gratefully acknowledge the beamline support at beamlines 7.3.3 and 11.0.1.2 provided by C. Wang, C. Zhu, and A.L.D. Kilcoyne. M. Ghasemi is acknowledged for the help with the SIMS training. X.Y. thanks Z. Peng, S. Stuard, and I. Angunawela for helping with the X-ray data acquisition.

Conflict of Interest

The authors declare no conflict of interest.

Keywords

additive, halogen-free solvents, mean-square composition variation, morphological aid, Nonfullerene polymer solar cells

Received: September 4, 2018
Revised: October 18, 2018
Published online: November 14, 2018

[1] F. C. Krebs, N. Espinosa, M. Hösel, R. R. Søndergaard, M. Jørgensen, *Adv. Mater.* **2014**, *26*, 29.
[2] J. Zhao, Y. Li, G. Yang, K. Jiang, H. Lin, H. Ade, W. Ma, H. Yan, *Nat. Energy* **2016**, *1*, 15027.
[3] a) Y. Diao, Y. Zhou, T. Kurosawa, L. Shaw, C. Wang, S. Park, Y. Guo, J. A. Reinspach, K. Gu, X. Gu, B. C. K. Tee, C. Pang, H. Yan, D. Zhao, M. F. Toney, S. C. B. Mannsfeld, Z. Bao, *Nat. Commun.* **2015**, *6*, 7955; b) H. W. Ro, J. M. Downing, S. Engmann, A. A. Herzing, D. M. DeLongchamp, L. J. Richter, S. Mukherjee, H. Ade, M. Abdelsamie, L. K. Jagadamma, A. Amassian, Y. Liu, H. Yan, *Energy Environ. Sci.* **2016**, *9*, 2835; c) F. Liu, S. Ferdous, E. Schaible, A. Hexemer, M. Church, X. Ding, C. Wang, T. P. Russell, *Adv. Mater.* **2015**, *27*, 886.
[4] L. Ye, Y. Xiong, H. Yao, A. Gadisa, H. Zhang, S. Li, M. Ghasemi, N. Balar, A. Hunt, B. T. O'Connor, J. Hou, H. Ade, *Chem. Mater.* **2016**, *28*, 7451.
[5] S. Zhang, L. Ye, H. Zhang, J. Hou, *Mater. Today* **2016**, *19*, 533.
[6] a) L. Ye, Y. Xiong, Q. Zhang, S. Li, C. Wang, Z. Jiang, J. Hou, W. You, H. Ade, *Adv. Mater.* **2018**, *30*, 1705485; b) X. Gu, Y. Zhou, K. Gu, T. Kurosawa, Y. Guo, Y. Li, H. Lin, B. C. Schroeder, H. Yan, F. Molina-Lopez, C. J. Tassone, C. Wang, S. C. B. Mannsfeld, H. Yan, D. Zhao, M. F. Toney, Z. Bao, *Adv. Energy Mater.* **2017**, *7*, 1602742.
[7] a) L. Ye, Y. Xiong, S. Li, M. Ghasemi, N. Balar, J. Turner, A. Gadisa, J. Hou, B. T. O'Connor, H. Ade, *Adv. Funct. Mater.* **2017**, *27*, 1702016; b) Y. Lin, Y. Jin, S. Dong, W. Zheng, J. Yang, A. Liu, F. Liu, Y. Jiang,

T. P. Russell, F. Zhang, F. Huang, L. Hou, *Adv. Energy Mater.* **2018**, *8*, 1701942; c) A. Wadsworth, R. S. Ashraf, M. Abdelsamie, S. Pont, M. Little, M. Moser, Z. Hamid, M. Neophytou, W. M. Zhang, A. Amassian, J. R. Durrant, D. Baran, I. McCulloch, *ACS Energy Lett.* **2017**, *2*, 1494.

[8] J. Czolk, D. Landerer, M. Koppitz, D. Nass, A. Colsmann, *Adv. Mater. Technol.* **2016**, *1*, 1600184.

[9] J. Hou, O. Inganäs, R. H. Friend, F. Gao, *Nat. Mater.* **2018**, *17*, 119.

[10] Y. Lin, J. Wang, Z. G. Zhang, H. Bai, Y. Li, D. Zhu, X. Zhan, *Adv. Mater.* **2015**, *27*, 1170.

[11] Y. Lin, F. Zhao, Q. He, L. Huo, Y. Wu, T. C. Parker, W. Ma, Y. Sun, C. Wang, D. Zhu, A. J. Heeger, S. R. Marder, X. Zhan, *J. Am. Chem. Soc.* **2016**, *138*, 4955.

[12] a) S. Li, L. Ye, W. Zhao, S. Zhang, S. Mukherjee, H. Ade, J. Hou, *Adv. Mater.* **2016**, *28*, 9423; b) Z. Liu, Y. Wu, Q. Zhang, X. Gao, *J. Mater. Chem. A* **2016**, *4*, 17604.

[13] L. Ye, H. Hu, M. Ghasemi, T. Wang, B. A. Collins, J.-H. Kim, K. Jiang, J. H. Carpenter, H. Li, Z. Li, T. McAfee, J. Zhao, X. Chen, J. L. Y. Lai, T. Ma, J.-L. Bredas, H. Yan, H. Ade, *Nat. Mater.* **2018**, *17*, 253.

[14] J. Song, M. Zhang, M. Yuan, Y. Qian, Y. Sun, F. Liu, *Small Methods* **2018**, *2*, 1700229.

[15] L. Lu, M. A. Kelly, W. You, L. Yu, *Nat. Photonics* **2015**, *9*, 491.

[16] N. Gasparini, X. Jiao, T. Heumueller, D. Baran, G. J. Matt, S. Fladischer, E. Spiecker, H. Ade, C. J. Brabec, T. Ameri, *Nat. Energy* **2016**, *1*, 16118.

[17] J. Li, C. W. Rochester, I. E. Jacobs, E. W. Aasen, S. Friedrich, P. Stroeve, A. J. Moulé, *Org. Electron.* **2016**, *33*, 23.

[18] X. Han, Z. Wu, B. Sun, *Org. Electron.* **2013**, *14*, 1116.

[19] Z. Shang, T. Heumueller, R. Prasanna, G. F. Burkhard, B. D. Naab, Z. Bao, M. D. McGehee, A. Salleo, *Adv. Energy Mater.* **2016**, *6*, 1601149.

[20] Y. Zhang, H. Zhou, J. Seifter, L. Ying, A. Mikhailovsky, A. J. Heeger, G. C. Bazan, T.-Q. Nguyen, *Adv. Mater.* **2013**, *25*, 7038.

[21] H. Yan, J. G. Manion, M. Yuan, F. P. García de Arquer, G. R. McKeown, S. Beaupré, M. Leclerc, E. H. Sargent, D. S. Seferos, *Adv. Mater.* **2016**, *28*, 6491.

[22] a) X. Jiao, L. Ye, H. Ade, *Adv. Energy Mater.* **2017**, *7*, 1700084; b) S. Mukherjee, C. M. Proctor, G. C. Bazan, T. Q. Nguyen, H. Ade, *Adv. Energy Mater.* **2015**, *5*, 1500877; c) S. Mukherjee, C. M. Proctor, J. R. Tumbleston, G. C. Bazan, T.-Q. Nguyen, H. Ade, *Adv. Mater.* **2015**, *27*, 1105.

[23] D. Baran, R. S. Ashraf, D. A. Hanifi, M. Abdelsamie, N. Gasparini, J. A. Röhr, S. Holliday, A. Wadsworth, S. Lockett, M. Neophytou, C. J. M. Emmott, J. Nelson, C. J. Brabec, A. Amassian, A. Salleo, T. Kirchartz, J. R. Durrant, I. McCulloch, *Nat. Mater.* **2016**, *16*, 363.

[24] D. Baran, N. Gasparini, A. Wadsworth, C. H. Tan, N. Wehbe, X. Song, Z. Hamid, W. Zhang, M. Neophytou, T. Kirchartz, C. J. Brabec, J. R. Durrant, I. McCulloch, *Nat. Commun.* **2018**, *9*, 2059.

[25] H. Yan, J. G. Manion, M. Yuan, F. P. Garcia de Arquer, G. R. McKeown, S. Beaupre, M. Leclerc, E. H. Sargent, D. S. Seferos, *Adv. Mater.* **2016**, *28*, 6491.

[26] F. Fabregat-Santiago, G. Garcia-Belmonte, I. Mora-Sero, J. Bisquert, *Phys. Chem. Chem. Phys.* **2011**, *13*, 9083.

[27] H. Kurt, C. W. Ow-Yang, *Phys. Status Solidi A* **2016**, *213*, 3165.

[28] E.-P. Yao, C.-C. Chen, J. Gao, Y. Liu, Q. Chen, M. Cai, W.-C. Hsu, Z. Hong, G. Li, Y. Yang, *Sol. Energy Mater Sol. Cells* **2014**, *130*, 20.

[29] C.-C. Chen, B.-C. Huang, M.-S. Lin, Y.-J. Lu, T.-Y. Cho, C.-H. Chang, K.-C. Tien, S.-H. Liu, T.-H. Ke, C.-C. Wu, *Org. Electron.* **2010**, *11*, 1901.

[30] G. Garcia-Belmonte, A. Guerrero, J. Bisquert, *J. Phys. Chem. Lett.* **2013**, *4*, 877.

[31] G. Garcia-Belmonte, P. P. Boix, J. Bisquert, M. Sessolo, H. J. Bolink, *Sol. Energy Mater Sol. Cells* **2010**, *94*, 366.

[32] B. J. Leever, C. A. Bailey, T. J. Marks, M. C. Hersam, M. F. Durstock, *Adv. Energy Mater.* **2012**, *2*, 120.

[33] L. J. A. Koster, V. D. Mihailetchi, R. Ramaker, P. W. M. Blom, *Appl. Phys. Lett.* **2005**, *86*, 123509.

[34] S. R. Cowan, A. Roy, A. J. Heeger, *Phys. Rev. B* **2010**, *82*, 245207.

[35] J. Lorrmann, B. H. Badada, O. Inganas, V. Dyakonov, C. Deibel, *J. Appl. Phys.* **2010**, *108*.

[36] G. Dennler, A. J. Mozer, G. Juska, A. Pivrikas, R. Osterbacka, A. Fuchsbauer, N. S. Sariciftci, *Org. Electron.* **2006**, *7*, 229.

[37] A. J. Mozer, G. Dennler, N. S. Sariciftci, M. Westerling, A. Pivrikas, R. Osterbacka, G. Juska, *Phys. Rev. B* **2005**, *72*, 035217.

[38] B. Philippa, C. Vijila, R. D. White, P. Sonar, P. L. Burn, P. Meredith, A. Pivrikas, *Org. Electron.* **2015**, *16*, 205.

[39] A. Hexemer, W. Bras, J. Glossinger, E. Schaible, E. Gann, R. Kirian, A. MacDowell, M. Church, B. Rude, H. Padmore, *J. Phys.: Conf. Ser.* **2010**, *247*, 012007.

[40] F. Liu, M. A. Brady, C. Wang, *Eur. Polym. J.* **2016**, *81*, 555.

[41] E. Gann, A. T. Young, B. A. Collins, H. Yan, J. Nasiatka, H. A. Padmore, H. Ade, A. Hexemer, C. Wang, *Rev. Sci. Instrum.* **2012**, *83*, 045110.

[42] S. C. Price, A. C. Stuart, L. Yang, H. Zhou, W. You, *J. Am. Chem. Soc.* **2011**, *133*, 4625.

[43] A. Pivrikas, N. S. Sariciftci, G. Juška, R. Österbacka, *Prog. Photovoltaics* **2007**, *15*, 677.